

*Cascade dc/dc Converters for Efficiency
Improvement and low Harmonic Content:
Experimental Validation*

*Convertidores dc/dc en Cascada para Incremento
de Eficiencia y Reducción de Contenido Armónico:
Validación Experimental*

Laura Cristina Paniagua Palacio

*Ingeniera Electricista
Universidad Nacional de Colombia
laurac.paniagua@gmail.com*

Iván José Ramírez Álvarez

*Ingeniero Electricista
Universidad Nacional de Colombia
godramirez@gmail.com*

Carlos Andrés Ramos Paja

*Ingeniero electrónico, Master en Automática, Doctor en Electrónica de Potencia
Universidad Nacional de Colombia
caramosp@unal.edu.co*

Recibido Mayo 05 de 2011 – Aceptado Noviembre 30 de 2011

ABSTRACT

This paper presents the experimental validation of the benefits provided by the cascade configuration of dc/dc converters over classical single dc/dc converters. The results obtained prove that the cascade connection of dc/dc converters, despite insert additional parasitic resistances, improves the voltage conversion ratio and efficiency of a step-up conversion chain. In addition, the adopted cascade configuration also reduces the current harmonics injected to sensible power sources like fuel cells or photovoltaic generators. Finally, a simple procedure to experimentally identify the inductor parasitic loss resistance on boost converters was also introduced.

Key Words: DC/DC converter, boost converter, efficiency, current harmonics.

RESUMEN

Este artículo presenta la validación experimental de los beneficios ofrecidos por la conexión en cascada de convertidores dc/dc sobre los convertidores dc/dc clásicos. Los resultados obtenidos prueban que la conexión en cascada de convertidores dc/dc, a pesar de insertar resistencias parásitas adicionales, incrementa la relación de transformación de voltaje y la eficiencia de un sistema de conversión. Además, la configuración en cascada seleccionada reduce el contenido armónico inyectado a fuentes de potencia sensibles como pilas de combustible y paneles fotovoltaicos. Finalmente, se presenta un procedimiento simple para identificar experimentalmente la resistencia parásita del inductor en un convertidor elevador.

Palabras clave: convertidor dc/dc, convertidor elevador, eficiencia, armónicos.

1. INTRODUCTION

Fuel cells and photovoltaic panels are the most attractive energy sources to contribute in the reduction of fossil-based fuels(W.A. Surdoval, Singhal et al. 2001), this based on its renewable sources and pollution free operation. But such options require the development of new power converters and control strategies to efficiently extract the required energy, placing the power generator at its most efficient operating point(Krein, Balog et al. 2004; Cabal, Alonso et al. 2007) . In particular, it is widely known that the current harmonics generated by the use of traditional power converters can seriously affect the fuel cell integrity(Haynes and Wepfer 2001). As for the photovoltaic applications, the current harmonics affect the detection of the best operating condition, reducing the system efficiency(Grandi, Casadei et al. 2003).

Such problems were addressed in the work “A Ripple-Mitigating Pre-filter Based on Interleaved DC-DC Boost Converters”, developed by the authors, which appeared in the 36th Annual Conference of the IEEE Industrial Electronics Society (IECON-2010, ©2010 IEEE)(Ramos-Paja, Carrejo et al. 2010), where only simulation results were provided. The solution proposed in(Ramos-Paja, Carrejo et al. 2010)was based on analyze the main harmonic content in the power converter through the current ripple injected to the source, and to develop a power conversion system able to filter the current harmonics generated during the converter

switching, which is traditionally addressed by the typical capacitor-filtering solution (Jang, Won et al. 2007). The strategy consist in parallelize two dc/dc switching converters to mitigate the current harmonics injected into the power source, and connect in cascade such dual converter with a single dc/dc converter, improving in this way the overall system efficiency in comparison with a single dc/dc converter solution.

This paper is intended to develop the prototypes and perform the experimental validations to prove the benefits of the cascade connection of dc/dc converters over single converters operation in terms of efficiency and current harmonics injection. Such efficiency improvement is interesting to demonstrate since a cascade converters connection introduces additional parasitic resistances in contrast with single converters. The paper is organized as follows: Section 2 describes the procedure to experimentally parameterize the boost converter model, which is required for the models comparison. Section 3 presents the experimental results to validate the improvements of the cascade connection of dc/dc converter over traditional single converters. Finally, the conclusions of the work are given in section 4.

2. BOOST CONVERTER EXPERIMENTAL MODEL PARAMETERIZATION

A boost converter can be designed depending on the input-output current-voltage requirements of the application, but it is necessary to take into account the voltage drop generated by the parasitic converter losses, where the dominant losses resistance corresponds to the inductor one, as depicted in figure 1. In this way, using the charge and volt-second balances (Erickson and Maksimovic 2001), eq. (1) presents the voltage conversion ratio of a boost converter considering a parasitic resistance R_L on the inductor, where D represents the converter duty cycle, R the load impedance, V_g the input voltage, and V the output voltage. Similarly, eq. (2) presents the steady-state inductor current I_L that flows through the parasitic resistance R_L causing ohmic losses, thus degrading the system efficiency. From such equations, the boost converter efficiency is given by (3).

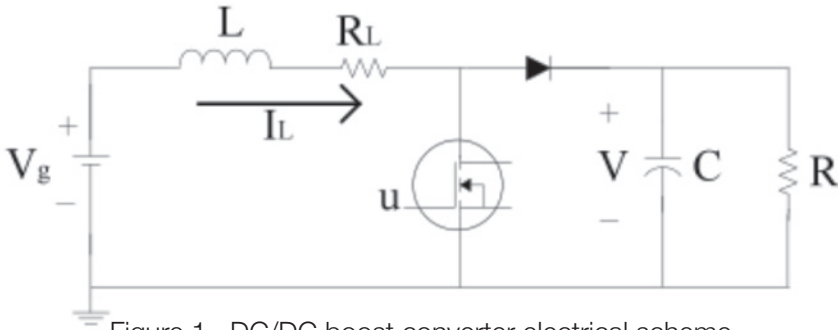


Figure 1. DC/DC boost converter electrical scheme

$$\frac{V}{V_g} = M(D) = \frac{1}{(1-D)} \frac{1}{\left(1 + \frac{R_L}{(1-D)^2 R}\right)} \quad (1)$$

$$I_L = \frac{V_g}{R(1-D)^2 + R_L} \quad (2)$$

$$\eta_F = \frac{1}{1 + \left(\frac{R_L}{(1-D)^2 R}\right)} \quad (3)$$

Another important design parameters concern the input current ripple, given in (4), where T is the switching period, L the inductor, and C the capacitor. The input current ripple must be carefully designed depending on the power source requirements since it can cause damages or power losses, i.e. large current ripples can damage fuel cells membranes (Ramos-Paja, Bordons et al. 2009) or produce high power losses in photovoltaic systems (Aranda, Galan et al. 2009).

$$\Delta I_L = \frac{V_g DT}{2L} \left(1 - \frac{R_L}{R(1-D)^2 + R_L}\right) \quad (4)$$

The previous equations describe the converter electrical operation and efficiency, but such relations depend on converter parameters which nominal values can be measured: the input and output voltages, and the load impedance and converter duty cycle, which ones are defined by the application. Moreover, the previous equations also strongly depend on the inductor parasitic resistance, which changes with the switching frequency

and inductor current (Yu, Holmes et al. 2002), therefore a simple procedure to estimate such a resistance is presented in the following subsections.

2.1. Experimental prototype

To illustrate the converter efficiency behavior and the inductor parasitic resistance estimation, the experimental prototype depicted in figure 2 was developed considering an input voltage $V_g = 5$ V, and output voltage $V = 36$ V, a 20 kHz switching frequency, and a maximum output current of 5 A. The inductor was selected to ensure a Continuous Conduction Mode (CCM) operation for 90 % of the converter power range (Erickson and Maksimovic 2001), using a 2300HT-221-RC (BOURNS) inductor of 220 μ H. The capacitors were designed to provide a voltage ripple lower than 10 % of the DC component, using EPOCS Metallized Polyester Film Capacitors of 47 μ F and 63 V.

Moreover, the diode and Mosfet adopted were the Schottky VS-20TQ045PBF-ND with a voltage drop of 0.51 V, and the N-channel STW55NE10, respectively. In addition, a CAS 6-NP current sensor was used to measure the inductor current.

Figure 3 shows the waveforms of the inductor current and Mosfet gate voltage for a steady-state duty cycle of 50 %. Such a figure shows that the ON time of the Mosfet is 25 μ s, which corresponds to the half of the switching period since the switching frequency is 20 kHz. In addition, the current waveform exhibits a phase delay of 180° introduced by the current sensor conditioning circuitry.

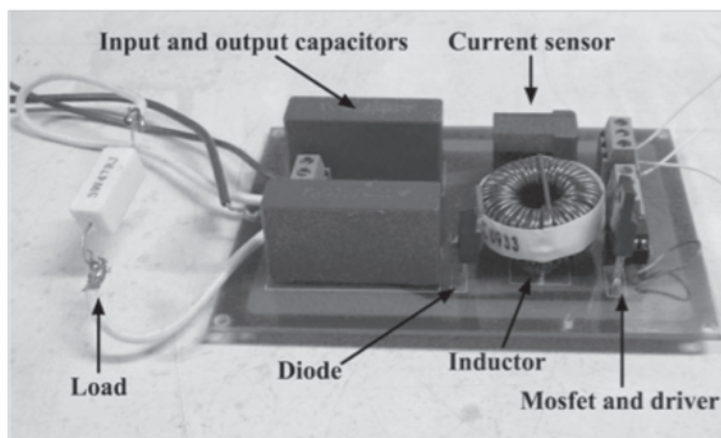


Figure 2. Experimental dc/dc boost converter

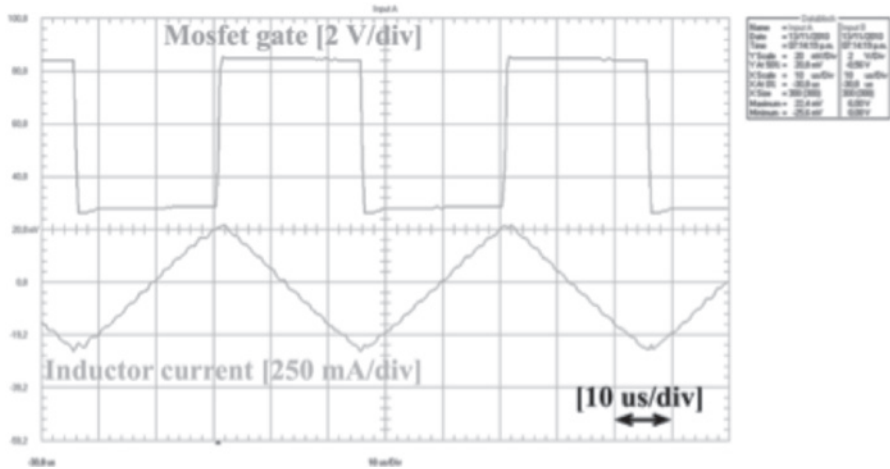


Figure 3. Experimental inductor current and Mosfet gate waveforms

The experimental voltage conversion ratio is presented in figure 4, where load resistances of 30 Ω and 45 Ω have been considered adopting an input voltage equal to 5 V for duty cycles between 0 % and 95 %. Such results are in agreement with the theoretical predictions of eq. (1), where the maximum voltage conversion ratio increases for a load impedance increment. Finally, for duty cycles lower than 60 % the converter experimental behavior is close to the ideal case $V/V_g = 1/(1-D)$ (Erickson and Maksimovic 2001). Figure 5 presents the experimental efficiency of the prototype, following the predictions of eq. (3): increments in the duty cycle generate decrements on the converter efficiency, while increments on the load impedance also increase the efficiency. Finally, the prototype exhibits electrical efficiencies higher than 80 % for duty cycles lower than 70 %.

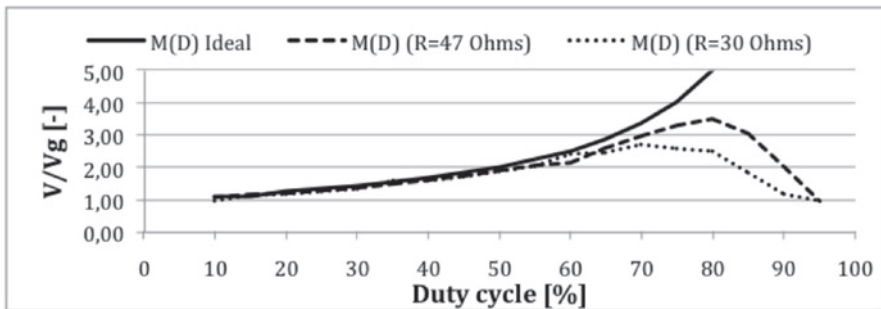


Figure 4. Experimental voltage conversion ratio for $V_g = 5V$

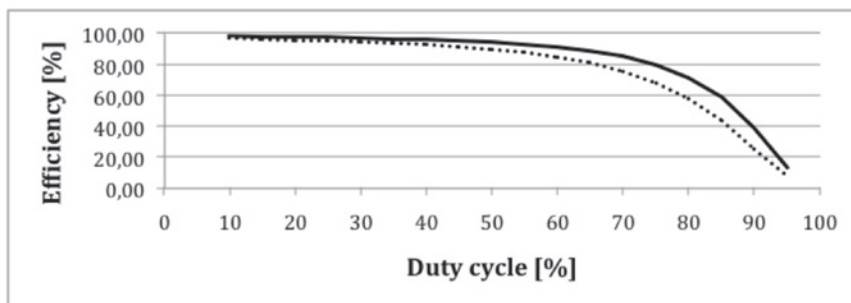


Figure 5. Experimental efficiency for $V_g = 5$ V (solid 47Ω , dotted 30Ω)

2.2 Calculation of inductor parasitic resistance

Since the inductor parasitic resistance strongly impacts both voltage conversion ratio and efficiency, it must be accurately calculated to properly model the converter. This can be done by applying duty cycle sweeps similar to experiments in figure 4 and use eq. (1) to accurately calculate the R_L/R factor. Figure 6 presents the experiments performed to determine R_L for different input voltage and load impedance conditions: eq. (2) has been parameterized using the converter components nominal values, and using a curve fitting software the R_L/R factors and R_L values reported in table 1 have been calculated. It is noted that the theoretical curves follow the experimental results for more than 80 % of the points, where the differences at the maximum power conditions, i.e. high output voltage in constant resistance conditions, are caused by the switching losses. Moreover, it is noted that the inductor parasitic resistance grows for increments on the input voltage, i.e. output power for constant load impedance and duty cycle. Finally, R_L can be estimated using the presented method to provide a more accurate boost converter model.

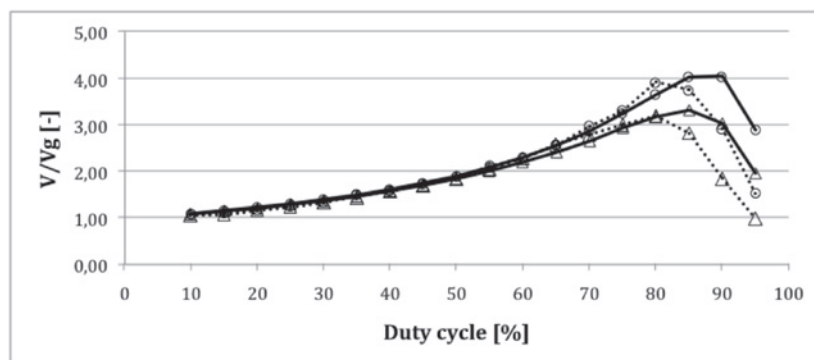


Figure 6. Inductor parasitic resistance calculation
(Solid: experiment, dotted: model, O: 47Ω , D: 30Ω)

Table 1. Estimation of the Inductor parasitic resistance

$V_g = 3 \text{ V}$	$R_L/R [-]$	$R_L [\Omega]$	$V_g = 5 \text{ V}$	$R_L/R [-]$	$R_L [\Omega]$
$R = 30 \Omega$	0,0230	0,6969	$R = 30 \Omega$	0,029	0,8787
$R = 47 \Omega$	0,0148	0,7015	$R = 47 \Omega$	0,016	0,7584

3. CASCADE OPERATION FOR EFFICIENCY IMPROVEMENT

In the theoretical work presented in (Ramos-Paja, Carrejo et al. 2010) was proposed that the cascade interconnection of multiple boost converters improves the overall system efficiency. Figure 7 presents the electrical scheme of the power conversion chain proposed in (Ramos-Paja, Carrejo et al. 2010), which is composed of a pre-amplifier intended to operate in cascade with a classical boost converter.

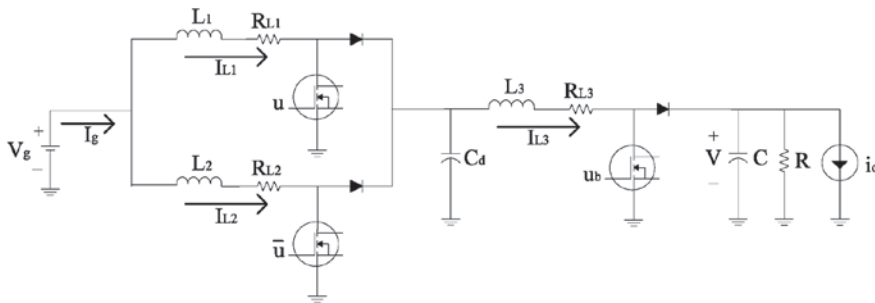


Figure 7. Cascade DC/DC boost converters electrical scheme

Adopting the condition of equal inductors for the pre-amplifier $R_{L1} \approx R_{L2} \approx R_L$, the voltage conversion ratio of the complete conversion chain is given by (5), and its steady-state input current is given by (6). Finally, eq. (7) summarizes the complete chain efficiency. From eqs. (1) and (5) is noted that the complete conversion chain provides higher voltage conversion ratio for the same parasitic power losses, and from eqs. (3) and (7) is noted that the efficiency is also improved (Ramos-Paja, Carrejo et al. 2010).

$$\frac{V}{V_g} = M(D) = \frac{2(1-D)R}{(1-D)^2 R + R_{L3} + 2R_L} \tag{5}$$

$$I_g = \frac{V}{R(1-D)} \left(\frac{1}{0,5 + \frac{R_L}{R}} \right) \quad (6)$$

$$\eta_F = \frac{1}{1 + \left(\frac{R_{L3}}{(1-D)^2 R} \right) + \left(\frac{2R_L}{(1-D)^2 R} \right)} \quad (7)$$

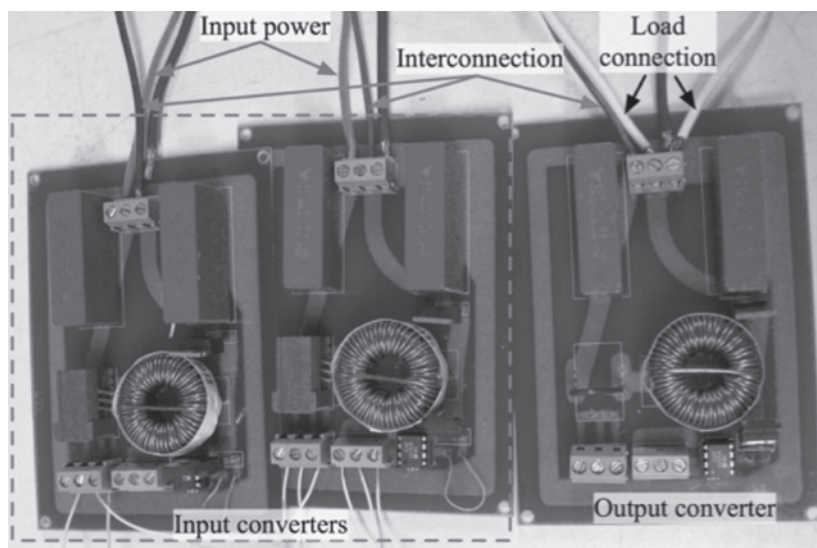


Figure 8. Experimental cascade dc/dc boost converters

The cascade connection of the boost converters of figure 7 was implemented as depicted in figure 8, where the yellow cables connect the power source with the input converters, the blue cables connect such converters with the output boost converter, the green cables connect the conversion chain to the ground, and the white cables connect the output converter with the load. In this case two signal generators were used: the first one generates the 50 % duty cycle for the pre-amplifier, and the second one generates the variable duty cycle for the cascade boost converter.

Figure 9 shows the experimental comparison between the cascade configuration and the classical boost converter for a 47 Ω load impedance, considering an input voltage $V_g = 5$ V and duty cycles between 10 % and 90 %. It is noted that the complete conversion chain provides higher output voltage for the same input voltage and duty cycle than the single

boost converter case. Such results prove that the cascade connection of dc/dc converters, despite insert additional parasitic resistances, improves the voltage conversion ratio of a step-up conversion chain, validating the theoretical predictions of (Ramos-Paja, Carrejo et al. 2010).

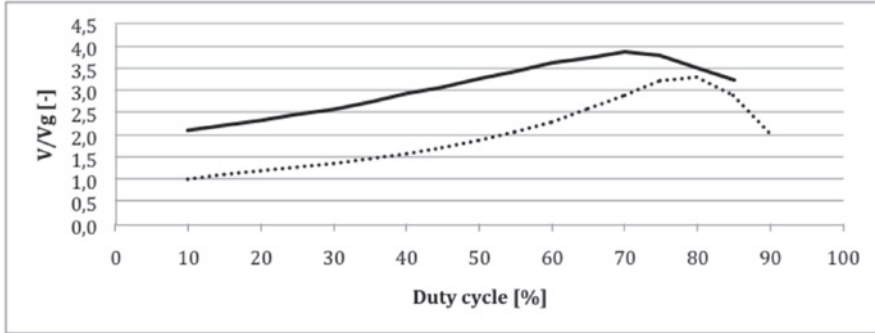


Figure 9. Experimental voltage conversion ratio (Solid: cascade configuration, dotted: single boost converter)

Similarly, an efficiency comparison between the cascade connection solution and the classical boost converter, for a 47Ω load condition, was experimentally performed. The results are presented in figure 10, where it is contrasted the prototypes efficiency, in terms of the output and input power ratio, and voltage conversion ratios. It is noted that the cascade connection provides higher efficiency for the same voltage conversion ratio, which is typically imposed by the application. Moreover, the complete conversion chain also provides higher voltage conversion ratio, therefore a higher load voltage is achievable. Such results prove that the cascade connection of dc/dc converters improves the efficiency of a step-up conversion chain, validating the theoretical predictions of (Ramos-Paja, Carrejo et al. 2010).

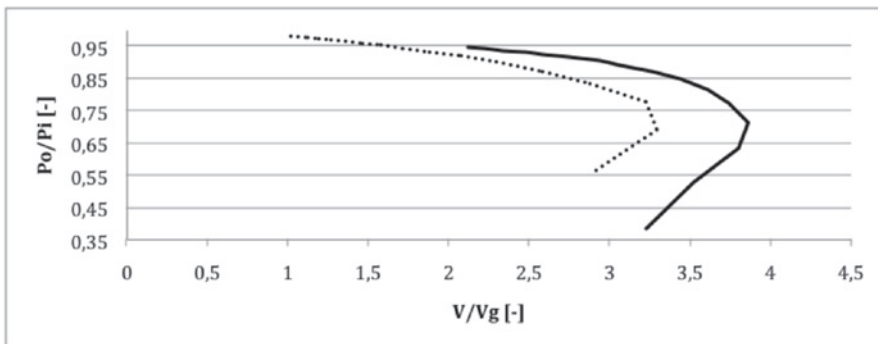


Figure 10. Experimental efficiency (Solid: cascade configuration, dotted: single boost converter)

Another important characteristic of the solution proposed in (Ramos-Paja, Carrejo et al. 2010) concerns the mitigation of the current ripple generated by the classical boost converter. Such a condition is achieved due to the complementary inductors current waveforms on the pre-amplifier, since both boost converters are driven by complementary signals applied to the Mosfets. Figure 11 presents the experimental waveforms of the inductors and input current in the cascade converters connection, where the complementary behavior is observed. In addition, such an experiment also presents the ripple-free input current I_g , where it is evident the small current harmonics injected to the power source, validating in this way the theoretical analyses presented in (Ramos-Paja, Carrejo et al. 2010).

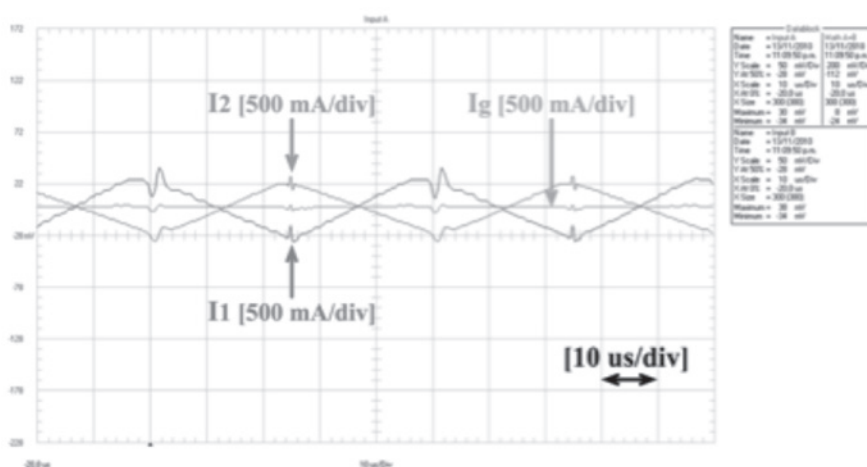


Figure 11. Input current ripples for the cascade converters connection solution

Similarly, the DC Total Harmonic Distortions (THD) for both the cascade converters connection and the classical boost input currents have been calculated from experimental measurements. The DC THD was calculated as (8), where h_i represents the current harmonics and h_0 the DC component. Figure 12 presents the experimental THD for both solutions, where it is observed again the significantly reduction in the current harmonics provided by the complete conversion chain over the classical solution.

$$THD = \frac{1}{h_0} \sum_{i=1}^{\infty} h_i \quad (8)$$

4. CONCLUSIONS

This paper has presented the experimental validation of the benefits provided by the cascade configuration of dc/dc converters over classical single dc/dc converters. Such a validation was performed by means of three dc/dc boost converters designed to operate alone or in cascade configurations. Moreover, a simple procedure to experimentally identify the inductor parasitic loss resistance on boost converters was also introduced. Such a parasitic resistance is important since it strongly impacts the converter model.

Finally, the experiments have proved that the cascade configuration presented in figure 7 improves the efficiency over the classical configuration of figure 1. In addition, such cascade configuration also significantly reduces the current harmonics injected to sensible power sources, e.g. fuel cells or photovoltaic generators.

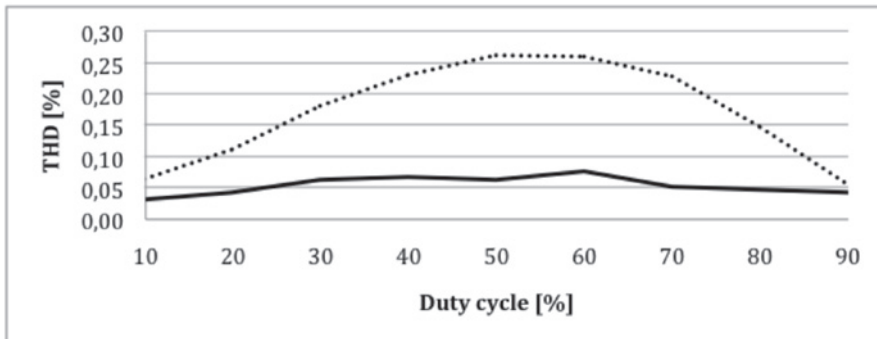


Figure 12. Experimental THD
(Solid: cascade configuration, dotted: single boost converter)

5. ACKNOWLEDGMENTS

This work was supported by GAUNAL and GITA research groups of the Universidad Nacional de Colombia under the projects SMART-ALEN and VECTORIAL-MPPT.

REFERENCES

- Aranda, E. D., J. A. G. Galan, et al. (2009). **Measuring the I-V Curve of PV Generators**. IEEE Industrial Electronics Magazine 3(3), pp. 4-14.

- Cabal, C., C. Alonso, et al. (2007). **Adaptive Digital MPPT Control for Photovoltaic Applications.** in IEEE International Symposium on Industrial Electronics, Vigo, Spain, pp. 2414-2419.
- Erickson, R. W. and D. Maksimovic. (2001). **Fundamentals of Power Electronics.** Springer
- Grandi, G., D. Casadei, et al. (2003). **Direct Coupling of Power Active Filters with Photovoltaic Generation Systems with Improved MPPT capability.** in IEEE Power Tech Conference, Bologna, pp. 23-26.
- Haynes, C. and W. J. Wepfer. (2001). **Characterizing Heat Transfer within a Commercial-grade Tubular Solid Oxide Fuel Cell for Enhanced Thermal Management.** International Journal of Hydrogen Energy 26(4), pp. 369-379.
- Jang, S. J., C. Y. Won, et al. (2007). **Fuel Cell Generation System with a new Active Clamping Current-fed Half-bridge Converter.** IEEE Transactions on Energy Conversion 22(2), pp. 332-340.
- Krein, P. T., R. S. Balog, et al. (2004). **High-frequency Link Inverter for Fuel Cells based on Multiple-carrier pwm.** IEEE Transactions on Power Electronics 19(5), pp. 1279-1288.
- Ramos-Paja, C. A., C. Bordons, et al. (2009). **Minimum Fuel Consumption Strategy for PEM Fuel Cells.** IEEE Transactions on Industrial Electronics 56(3), pp. 685-696.
- Ramos-Paja, C. A., C. Carrejo, et al. (2010). **A Ripple-mitigating Pre-filter Based on Interleaved DC-DC Boost Converters.** in 36th Annual Conference on IEEE Industrial Electronics Society, Glendale, pp. 2771-2777.
- W.A. Surdoval, S. C. Singhal, et al. (2001). **The Solid State Energy Conversion Alliance SECA.** in U.S. Department of Energy Initiative to Promote the Development of Mass Customized Solid Oxide Fuel Cells for Low-Cost Power, The 7th International Symposium on Solid Oxide Fuel Cells, Tsukuba, Japan, pp. 1-7.
- Yu, Q., T. W. Holmes, et al. (2002). **RF Equivalent Circuit Modeling of Ferrite-core Inductors and Characterization of Core Materials.** IEEE Transactions on Electromagnetic Compatibility 44(1), pp. 258-262.